16. R. J. Poreda, P. D. Jenden, I. R. Kaplan, H. Craig, *Geochim. Cosmochim. Acta* **50**, 2847 (1986).
17. H. A. Wollenberg, A. R. Smith, E. H. Bailey, *J. Geophys. Res.* **72**, 4139 (1967); F. C. W. Dodge, D. C. Ross, H. A. Wollenberg, A. R. Smith, *Geol. Soc. Am. Abstr.* **1**, 266 (1969).
18. The inability of a stained fluid to retain a residual magmatic signal assumes (i) a mantle He concentration in the stained fluid defined by the measured ^{3}He content of the Varian–Phillips well (9.52×10^{-16} mol/g), (ii) an initial stained fluid ^{3}He/^{4}He ratio of 8 Ra, (iii) a 5% average porosity, and (iv) a radiogenic ^{4}He release rate from the host rocks to the stained fluid equivalent to the production rate.
19. T. M. Johnson and D. J. DePaolo, *Water Resour. Res.* **30**, 1571 (1994). Implicit in the steady-state assumption is that the radiogenic ^{4}He accumulation rate in the fluid is equivalent to the production rate in the host rocks.
20. R. E. Wallace, in *The San Andreas Fault System, California*, R. E. Wallace, Ed. (U.S. Geological Survey, Washington, DC, 1990), professional paper 1515, p. 3.
21. P. Allard, *Geophys. Res. Lett.* **19**, 1479 (1992).
22. B. Marty and A. Jambon, *Earth Planet. Sci. Lett.* **83**, 16 (1987); T. Trull, S. Nadeau, F. Pineau, M. Polve, M. Javoy, *ibid.* **118**, 43 (1993).
23. J. D. Bredehoeft and S. E. Ingebritsen, in *The Role of Fluids in Crustal Processes*, J. D. Bredehoeft and D. L. Norton, Eds. (National Academy Press, Washington, DC, 1990), pp. 158–164.
24. R. C. Bailey, *Geophys. Res. Lett.* **17**, 1129 (1990).
25. P. Segall and J. R. Rice, *J. Geophys. Res.* **100**, 22155 (1995).
26. T. Atwater, *Bull. Geol. Soc. Am.* **81**, 3513 (1970); K. P. Furlong, W. D. Hugo, G. Zandt, *J. Geophys. Res.* **94**, 3100 (1989); J. Namson and T. L. Davis, *Bull. Geol. Soc. Am.* **100**, 257 (1988).
27. D. L. Jones, R. Graymer, C-Y. Wang, T. V. McEvilly, A. Lomax, *Tectonics* **13**, 561 (1994); B. M. Page and T. M. Brocher, *Geology* **21**, 635 (1993).
28. P. D. Jenden, I. R. Kaplan, R. J. Poreda, H. Craig, *Geochim. Cosmochim. Acta* **52**, 851 (1988).
29. B. Wernicke *et al.*, *Science* **271**, 190 (1996).
30. I. Barnes, R. W. Kistler, R. H. Mariner, T. S. Presser, in *U.S. Geological Survey Water-Supply Paper* (U.S. Geological Survey, Washington, DC, 1981), paper 2181, p. 1.
31. Y. K. Kharaka, F. A. Berry, I. Friedman, *Geochim. Cosmochim. Acta* **37**, 1899 (1973).
32. This work was partly supported by the Director, Office of Energy Research, Office of Basic Energy Sciences, Engineering, and Geosciences Division of the U.S. Department of Energy under contract DE-AC03-76SF00098.

24 January 1997; accepted 14 October 1997

Evolution of the Pacific-Antarctic Ridge South of the Udintsev Fracture Zone

Louis Géli,* Henri Bougault, Daniel Aslanian, Anne Briais, Laure Dosso, Joël Etoubleau, Jean-Pierre Le Formal, Marcia Maia, Hélène Ondréas, Jean-Louis Olivet, Chris Richardson, Keizo Sayanagi, Nobukazu Seama, Anjana Shah, Ivan Vlastelic, Michiko Yamamoto

Because of the proximity of the Euler poles of rotation of the Pacific and Antarctic plates, small variations in plate kinematics are fully recorded in the axial morphology and in the geometry of the Pacific-Antarctic Ridge south of the Udintsev fracture zone. Swath bathymetry and magnetic data show that clockwise rotations of the relative motion between the Pacific and Antarctic plates over the last 6 million years resulted in rift propagation or in the linkage of ridge segments, with transitions from transform faults to giant overlapping spreading centers. This bimodal axial rearrangement has propagated southward for the last 30 to 35 million years, leaving trails on the sea floor along a 1000-kilometer-long V-shaped structure south of the Udintsev fracture zone.

Because of its remoteness, the Pacific-Antarctic ridge (PAR) south of the Udintsev fracture zone (FZ) remained poorly known until the recent past (*1*). From satellite gravity data, it has been predicted (*2*) that morphological transitions occur along the ridge axis as the spreading rate increases with distance from the Euler pole of rotation between the Antarctic and Pacific plates: from 54 mm/year near 65°S up to 74 mm/year at its intersection with the Udintsev FZ, near 55°S (*3*). Satellite gravity data (*4*) also reveal a large-scale V-shaped structure that extends for more than 1000 km south of the Udintsev FZ and separates two domains (Fig. 1): one of rough sea floor, with many well-marked fracture zones as is typical of slow spreading centers, and one of smooth sea floor, as is typical of fast spreading centers. Sahabi *et al.* (*5*) proposed that this V-shaped structure may reflect a change in axial morphology south of the Udintsev FZ that progressively propagated southward during the last 30 million years (My). To analyze this region and test this hypothesis, the French research vessel (R/V) *L'Atalante* (*6*) explored an 1800-km-long section of the ridge, extending between 65°30′S, 174°40′W and the Udintsev FZ, in January and February of 1996 (Fig. 1).

The PAR south of the Udintsev FZ is divided into three domains of different morphological signatures (Fig. 2). The southern area, between 65°30′S, 174°40′W and 64°40′S, 172°W, has an axial, valley-type morphology similar to that observed at slow to intermediate spreading centers. The northern area, northeast of 63°10′S, 157°20′W, has an axial, dome-type morphology characteristic of fast spreading centers. In between, a transition zone extends for 800 km along the axis of the PAR.

In the south, the discontinuities separating the 80-km-long segments are curved and resemble overlapping spreading centers (OSCs) (Fig. 2). In the transitional domain, the ridge morphology alternates from a flat axial dome to a shallow axial valley, and most often the across-axis topographic relief is subtle. A large propagating rift (PR) is present near 167°20′W, 63°48′S (Fig. 3) and a second, smaller one near 63°15′S, 165°10′W. Both PRs appear to have initiated at the Heirtzler FZ. By extrapolating the pseudofault traces up to this FZ, we estimate that the large PR formed about 2.5 million years ago (Ma), and the younger one about 0.8 Ma. In the northern domain, an axial dome is present at an average depth of 2300 m. However, a rifted high region (near 57°S, for instance) that evolves into an axial graben (south of the 58°20′S OSC, for instance) appears in some places. The ridge axis is offset by three right-lateral transform faults (TFs): the Le Géographe TF near 62°10′S, the L'Astronome TF near 59°30′S, and the Saint-Exupéry TF near 57°30′S (*7*). The ridge axis is also interrupted by four left-lateral nontransform offsets, three OSCs near 62°30′S, 60°20′S, and 58°20′S, respectively, and one deviation of axial linearity near 57°10′S. Near 61°10′S, a nontransform offset can be inferred from satellite altimetry, but it was not covered during our cruise.

The variation in spreading rate con-

L. Géli, H. Bougault, J. Etoubleau, J.-P. Le Formal, H. Ondréas, J.-L. Olivet, I. Vlastelic, Institut Francais de Recherche pour l'Exploitation de la Mer (IFREMER), Boite Postale 70, 29280 Plouzané, France.
D. Aslanian and C. Richardson, Bullard Laboratories, University of Cambridge, Cambridge, CB3OEZ, UK.
A. Briais, Observatoire Midi-Pyrénnées, 18 Avenue Edouard Belin, 31055 Toulouse-Cédex, France.
L. Dosso, CNRS-IFREMER, Boite Postale 70, 29280 Plouzané, France.
M. Maia, Université de Bretagne Occidentale, 6 Avenue Le Gorgeu, 29285 Brest, France.
K. Sayanagi, Geological Survey of Japan, 1-1-3, Higashi, Tsukuba, Ibaraki, 305, Japan.
N. Seama and M. Yamamoto, Chiba University, 1-33, 263 Inage-Bu-Chiba, Chiba, Japan.
A. Shah, School of Oceanography, University of Seattle, Seattle, WA 98195, USA.

*To whom correspondence should be addressed.

trols the present-day axial morphology along the PAR: above a threshold spreading rate, the axial morphology changes from a valley to a high (5, 8). The transitional section between typical axial valley and axial high morphologies presently extends from 64°30′S to 62°30′S, and from the full spreading rates of 54 to 64 mm/year. However, although the spreading rate increases steadily from south to north, both types of axial morphologies alternate in the transitional section, suggesting that parameters other than just the spreading rate shape the axial relief locally. Trace element and isotopic ratios (9) of the basalts collected along the PAR vary little (Fig. 2), indicating that there is no hot spot influence in the area, and that even if heterogeneities in mantle temperature or composition play a role in controlling the axial morphology, this role is a second order effect.

The relative motions between the Pacific and the Antarctic plates (10) rotated counterclockwise from 70 to about 24 Ma (chron 6c), then remained constant between 24 and 12 Ma, and rotated clockwise since about 12 Ma (chron 5a). The spreading rate decreased from 70 to about 33 Ma, and increased since then, except in the period between chrons 6c and 5d (23 to 18 Ma), during which it decreased. For the late Neogene, Cande *et al.* (10) argued that changes in plate motions involve a mixture of gradual changes in direction, interspersed with sudden, sharp changes. For example, they document a sharp change at chron 3a (5.9 Ma) and two minor changes after chron 2a (2.58 Ma) and chron 1 (0.78 Ma) that are superim-

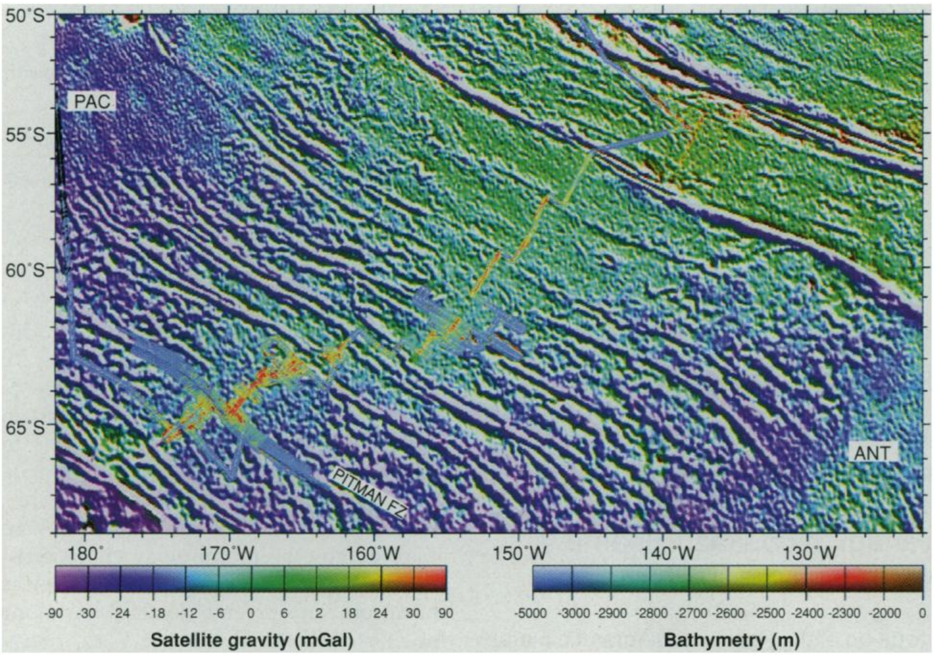

Fig. 1. Shaded relief image (north illumination) of shipboard bathymetry superimposed on satellite gravity data (4). White lines indicate the R/V *L'Atalante* track. The data along the Pitman FZ were acquired in 1992 with R/V *Maurice Ewing* (10). PAC, Pacific plate; ANT, Antarctic plate.

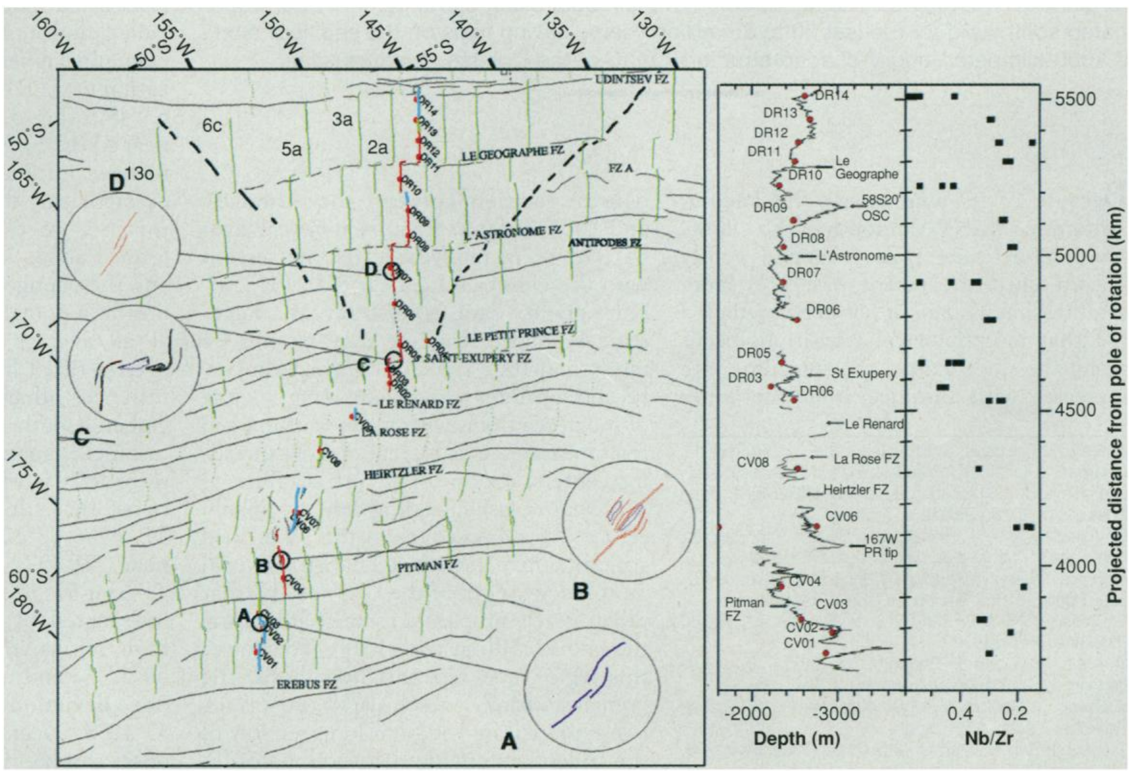

Fig. 2. Synthetic structural map of the area. Off-axis structures in areas without shipboard coverage are inferred from satellite gravity data (4). Sections of the PAR with an axial graben are in light blue; sections with an axial high are in red; those sections where the axial morphology is less pronounced are in green. The major characteristic types of axial discontinuities are detailed on insets. (**A**) Graben/graben OSC structure (for example, near 64°43′S, 172°15′W); (**B**) self decapitation structure (17) (for example, near 64°5′S, 168°45′W); (**C**) WFZs with bent "overshot ridges" (15) and an extensional basin within the TF (for example, near 62°30′S, 156°23′W); (**D**) dome/dome OSC structure like those found at the East Pacific Rise (17). Light green off-axis lines indicate isochrons 2a, 3a, 5a, 6c, and 13o, computed after (10). The along-axis plot on the right is expressed versus distance in kilometers from the Euler pole of rotation of the Pacific and Antarctic plates (there is no exact correspondence between distances in kilometers and the geographical map coordinates above). The left plot indicates axial bathymetry and location of rock samples (red dots). The right represents variations of the Nb/Zr ratio (9).

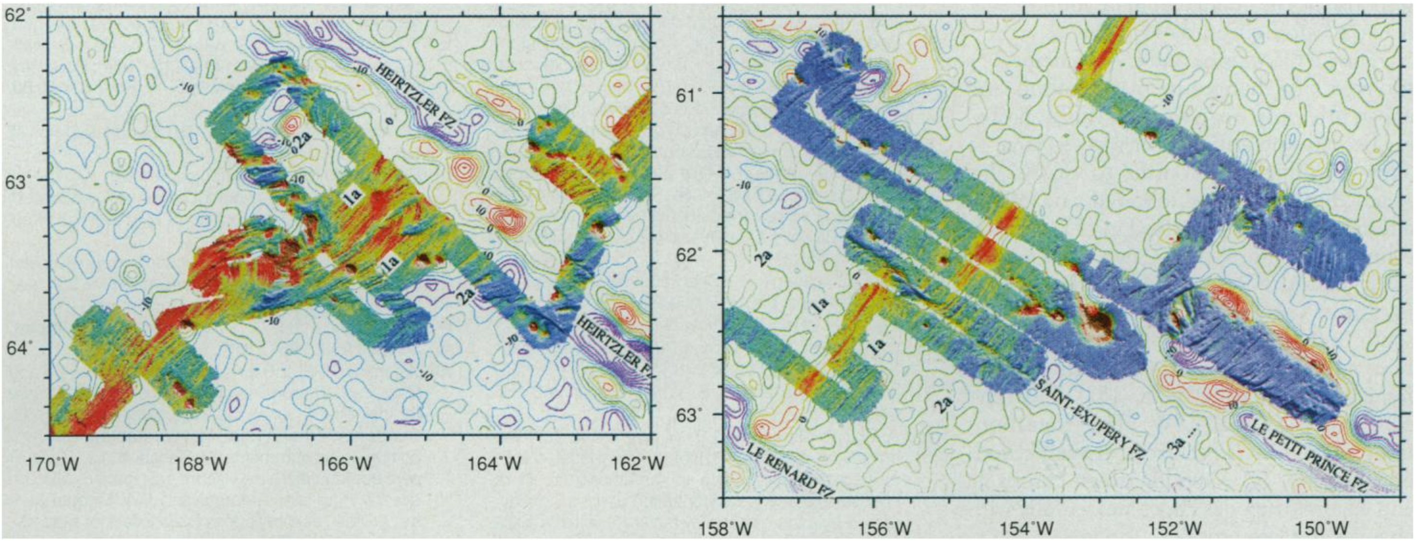

Fig. 3. Shaded relief image (southwest illumination) of sea floor bathymetry. The color scale (in meters) is the same as in Fig. 1. Color isolines in the background are satellite gravity 5-mGal isocontours. Dots indicate the location of magnetic isochrons 1a, 2a, and 3a. The left figure shows the area of the 167°20′W and 165°10′W PRs, and the right one, the tip of the large V-shaped structure.

posed on a gradual clockwise rotation over the last 12 My. These changes in spreading direction and rate have played a key role in shaping the axial morphology and the geometry of the plate boundary.

Indeed, the PRs along the PAR near 167°20′W and 165°10′W are likely to result from the latter changes in spreading direction, respectively at chrons 1 and 2a. Several mechanisms have been proposed to explain the existence of PRs along ridges: propagation due to lateral mantle flow away from hot spots (*11*), propagation of a ridge as a crack down a topographic slope (*12*), or the development of PRs to allow for a ridge reorientation (*13*). However, the nearest hot spot is very far away from this section of the PAR, and the crack model does not apply to the 167°W PR as straightforwardly as to other PRs such as the Galápagos and the Easter PRs (*12*). Because the age of inception of the PRs corresponds to that of the last two rotations of the spreading direction, we favor the third hypothesis.

The three 60-km offset TFs in the northern part of our study area are all characterized by one or two deep, rhomboidal basins with a main direction of 120°N, indicating recent (<3 Ma) extensional tectonics (*14*). On the ends of each basin, the axial crest of the PAR bends inward and becomes subparallel to the transform zone, wrapping over it about 20 km. In addition, the fossil traces of these wrapped FZs (WFZs) are shifted by about 10 km. Following Lonsdale (*15*), we infer that the special shape of the WFZs and the shift between the fossil traces may be attributed to extension resulting from the change in the Pacific-Antarctic plate motion that occurred shortly after chron 2a.

In the northern part of our survey area (between 61°S and 62°40′S), satellite gravity data indicate the presence of a FZ, named Le Petit Prince FZ (*7*), which does not appear on crust younger than about 4.5 to 5 Ma (Fig. 3, right). As the Le Petit Prince FZ is interrupted, a complex structure is observed in the bathymetry data in crust 3 to 4 My old, near 62°30′S, 152°W (*16*). This structure represents the fossil trace of a giant OSC, which formed just after the Le Petit Prince TF disappeared in

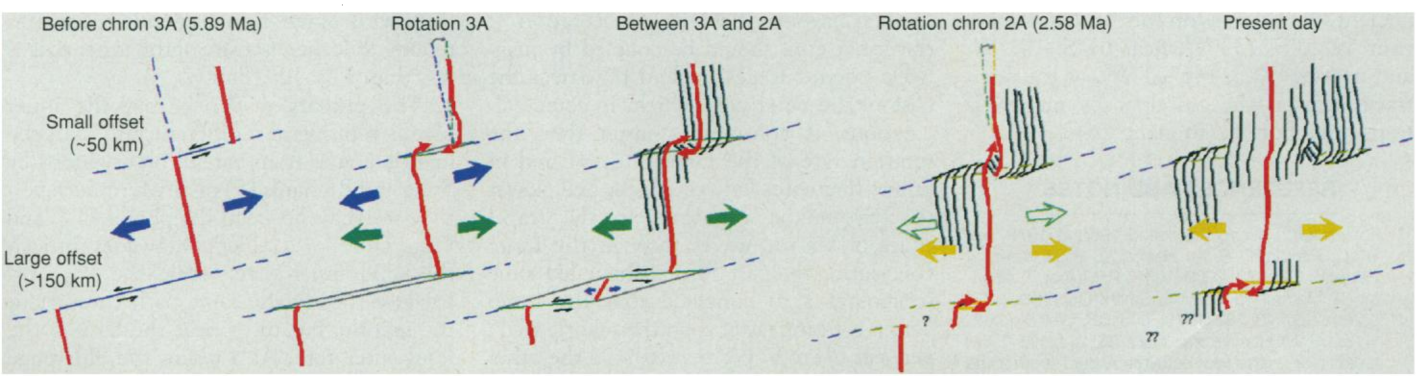

Fig. 4. Sketch describing how clockwise rotations of the spreading direction induced morphological reorganizations along the axis of the PAR south of the Udintsev FZ. Before chron 3a, two TFs are present: for instance, Le Petit Prince and Saint-Exupéry FZs, the first with a small offset (<50 km), and the second with a large offset (>150 km). At chron 3a, the spreading center rotates clockwise, resulting in an extensional zone in the transform zone and in an offset in the fossil traces of the FZ. Between chron 3a and 2a, the northern and the southern branches of the spreading centers "overshoot" (*15*) the basin of the small offset transform. The FZ becomes a WFZ or a giant OSC, depending on the initial offset of the transform and on the amount of rotation. In the large offset TF, the extensional zone is too large to be covered by the "overshot ridges," and the FZ evolves according to one of the three models described in (*15*). In the present case, the TF is split in two parts. At chron 2A, a second rotation decreases the distance between the two branches of the spreading center and permits their linkage in the north. In the south, the small offset of the newly formed FZ permits an evolution into a WFZ or into a giant OSC.

response to the change in plate motion that occurred after chron 3a (Fig. 4).

The Le Géographe and L'Astronome TFs survived the changes in plate motion and apparently only evolved into WFZs, probably because the initial offset was too large to allow the transition from FZ to GOSC. Instead, they may have followed one of the alternative models described in (*15*). On the other hand, the traces of two FZs (respectively named FZ A and Antipodes FZ) are interrupted at the boundary of the large V, south of the Udintsev FZ. At their intersection with the ridge axis, OSCs are present, respectively, near 60°11'S, 152°15'W and near 58°23'S, 148°40'W. The transitions from TFs to OSCs occurred between chrons 6c and 5d for FZ A, and between chrons 4a and 3a for Antipodes FZ, coincidentally with changes in plate motions.

The proximity of the Euler poles of rotation of the Pacific and the Antarctic plates and the fact that the spreading rate is close to the threshold value over most of the ridge length amplify the effects of the changes in plate motions. The increase in spreading rate and the clockwise change in the direction of the Pacific-Antarctic relative motion since 6 Ma have had three main consequences: (i) the axial morphology has changed from a rift valley to an axial high, (ii) rift propagation was triggered, and (iii) axial geometry has been rearranged, with the linkage of ridge segments and transitions from FZs to OSCs. Extrapolation of shipboard data interpretations suggests that this scheme has persisted over the last 30 to 35 My and explains most of the large V-shaped structure. This V, which initiated south of the Udintsev FZ shortly after chron 13o (33.5 Ma), results from a change in axial morphology that propagated southward. Its boundaries are the fossil traces of pseudofaults related to ancient PRs (such as on the Antarctic plate near 59°20'S, 132°W, near 61°S, 141°W, and near 61°30'S, 146°20'W), or the fossil traces left on the sea floor by numerous transitions from FZ to giant OSC.

REFERENCES AND NOTES

1. For research during the period 1960 to 1975, see W. C. Pitman III, E. M. Herron, J. R. Heirtzler, *J. Geophys. Res.* **73**, 2069 (1968); P. Molnar, T. Atwater, J. Mammerickx, S. M. Smith, *Geophys. J. R. Astron. Soc.* **40**, 383 (1975); and J. K. Weissel, D. E. Hayes, E. M. Herron, *Mar. Geol.* **25**, 231 (1977). For recent work with swath bathymetry data south of the Udintsev FZ, see (*10*) and A. Macario *et al.*, *J. Geophys. Res.* **99**, 17921 (1994).
2. C. Small and D. T. Sandwell, *J. Geophys. Res.* **97**, 3225 (1992).
3. C. DeMets, R. G. Gordon, D. F. Argus, S. Stein, *Geophys. J. R. Astron. Soc.* **101**, 425 (1990).
4. D. T. Sandwell and W. H. F. Smith, *Eos Trans. Am. Geophys. Union* **73**, 133 (1992).
5. M. Sahabi *et al.*, *Earth Planet. Sci. Lett.* **137**, 157 (1996).
6. R/V *L'Atalante* is equipped with a SIMRAD EM-12 dual multibeam echosounder system, a KSS-30 Bodenseewerk gravimeter, and a proton magnetometer. We also used a shipboard three-component magnetometer from Chiba University.
7. To avoid confusion, we do not use the old nomenclature (FZ VII, FZ VIII, and so on). The names Antipodes, Heirtzler, Pitman, Erebus, Terror, and Emerald FZ are after Cande *et al.* (*10*). The TFs Le Géographe, L'Astronome, Le Petit Prince, Saint-Exupéry, Le Renard, and La Rose are named after the French writer Antoine de Saint-Exupéry and the protagonists of his novel *Le Petit Prince.*
8. See, for example, Y. Chen and W. J. Morgan, *J. Geophys. Res.* **95**, 17571 (1990).
9. I. Vlastelic *et al.*, *Terra Nova* **9** (abstr.), 515 (1997).
10. S. C. Cande, C. A. Raymond, J. Stock, W. F. Haxby, *Science* **270**, 947 (1995).
11. J. M. Brozena and R. S. White, *Nature* **348**, 149 (1990).
12. J. Phipps-Morgan and E. M. Parmentier, *J. Geophys. Res.* **90**, 8603 (1985). In this model, the PR propagates like a crack in the lithosphere in response to a stress concentration at its tip, characterized by a stress intensity factor *K*. To estimate *K*, we used the expression (*1*) given by these authors for a symmetrically loaded, pressurized crack of length 2*L*. We predicted the off-axis sea floor topography from satellite gravity data and R/V *L'Atalante* multibeam data [J. Bastin, *Mémoire de fin d'Études* (École Polytechnique, Paris, 1996)]. Then, using the ridge axis and the 20-km off-axis topographic profiles, we found that $K > 0$ only if $L > 450$ km.
13. For example, see D. S. Wilson, R. N. Hey, C. Nishimura, *J. Geophys. Res.* **89**, 9215 (1984); R. N. Hey, H. W. Menard, T. M. Atwater, D. W. Caress, *ibid.* **93**, 2803 (1988).
14. D. Aslanian *et al.*, *Eos Trans. Am. Geophys. Union* **77** (abstr.), 729 (1996).
15. P. Lonsdale [*Marine Geophys. Res.* **16**, 105 (1994)] reported a curved, "overshot ridge" near the eastern ridge transform intersection of the 380-km offset Heezen TF.
16. The shipboard three-component magnetometer data indicate that the magnetization vector near 152°W, 62°30'S underwent a rotation.
17. K. C. Macdonald, D. S. Scheirer, S. M. Carbotte, *Science* **253**, 986 (1991).
18. We thank IFREMER for supporting our research and Captain G. Tredunit and the crew of R/V *L'Atalante* for their efforts during the Pacantarctic cruise. S. C. Cande made the EW9201 data available and provided numerous comments. M. Sahabi and J.-C. Sempéré contributed to the Pacantarctic project. Discussions with J. Phipps-Morgan and J. W. Morgan were helpful. L.G. acknowledges P. Lonsdale for a discussion before the Pacantarctic cruise; D.A. and C.R. wish to thank D. P. McKenzie. A.B. benefited from a grant from Institut National des Sciences de l'Univers. Figures 1 to 3 were made with GMT.

1 July 1997; accepted 7 October 1997

Inner Core Rotation Rate from Small-Scale Heterogeneity and Time-Varying Travel Times

Kenneth C. Creager

The time it takes seismic waves to propagate from South Atlantic earthquakes through the inner core to station COL in Alaska has decreased systematically over the past 30 years. Travel times from three earthquakes in 1991 to an array of 37 seismometers in Alaska suggest that lateral gradients in seismic wavespeeds are steep in this part of the inner core. This combination of observations can be explained by postulating that the inner core is rotating 0.2° to 0.3° per year faster than the mantle.

Numerical modeling of fluid flow in Earth's outer core has produced realistic models for the geodynamo that generates Earth's magnetic field (*1–4*). Rotation of the inner core should be coupled by magnetic Lorentz forces to fluid flow near the base of the outer core which, in some calculations, is consistently faster than the rotation rate of the mantle (*2*, *3*) and in others fluctuates between faster and slower (*4*). Systematic variations in the travel times of seismic waves through the inner core during the past 30 years have led some seismologists to conclude that the inner core is rotating faster than the mantle by 1° per year (*5*) to 3° per year (*6*). On the other hand, gravitational coupling between small aspherical variations in the topography of the inner core and in the density structure of the mantle are thought to prevent differential rotation between the inner core and mantle unless the inner core can deform its large-scale shape on time scales of years. To reconcile these fast differential rotation rates with gravitational coupling seems to require that the viscosity of the inner core is less than 3×10^{16} Pa·s (*7*, *8*).

The primary evidence that the inner core is rotating at a different rate than the mantle comes from careful observations by Song and Richards (*5*) of differential travel-time residuals between the phases P'_{BC} and P'_{DF}. The P'_{DF} (or PKP_{DF}) ray goes through the solid inner core, while the P'_{BC} ray traverses nearly the same path throughout the mantle, but turns near the base of the fluid outer core. As a result, the difference in travel times for these two rays is sensitive to the structure of the inner core but is much less sensitive to structure in the crust and mantle. Song and Richards found that the differential time residuals observed at station COL in Alaska from earthquakes near the South Sandwich Islands increase systematically by about 0.3 s as a function of

Geophysics Program, Box 351650, University of Washington, Seattle, WA 98195–1650, USA. E-mail: kcc@geophys.washington.edu